A Conformal Microwave Measurement System for Imaging Buried Anomalies

M Shifatul Islam[(1)], M Asiful Islam[(2)], and Asimina Kiourti[(1)]

[(1)] Dept. of Electrical and Computer Engineering, The Ohio State University, Columbus, OH 43212, USA
(islam.207@buckeyemail.osu.edu)

[(2)] Dept. of Electrical and Electronic Engineering, Bangladesh University of Engineering and Technology, Dhaka, Bangladesh

***Abstract*—Microwave imaging has long been reported for locating buried anomalies inside a bulk object as relying upon external measurements of microwave data. The approach is non-invasive, low-cost, portable, and the use of non-ionizing radiation makes it popular for biomedical applications. In this work, we explore the experimental feasibility of a conformal microwave imaging system, where the antennas are mounted on or very close to the imaging object. Our proof of concept setup entails 12 antennas surrounding a plastic cylindrical frame in free space with two dielectric cylinders used as anomalies. S-parameters were measured using a network analyzer and a 12-port switching matrix. For imaging, we used the Born Iterative Method, where the data equation was replaced with the S-parameter sensitivity formula. Simulation and measurement results show good quality image reconstruction, asserting the feasibility of the proposed conformal imaging setup. Future work will incorporate tissue-emulating materials to ultimately develop a stable and wearable imaging system.**

I. Introduction

Microwave imaging (MWI) involves the use of electromagnetic (EM) radiation in the microwave spectrum to obtain qualitative or quantitative information (i.e., images) of buried anomalies inside any domain. The method is non-invasive and has widespread geophysical and biomedical applications [1]–[3]. Notably, MWI devices are easy to build, data acquisition is straightforward, and the use of non-ionizing radiation assures safety.

In traditional MWI, the transmitter and receivers are placed sufficiently far from the objects to ensure the data acquisition domain and the object domain are separated [4]. However, for conformal imaging systems, these two domains will overlap. Though such setups have been explored in simulations, experimental validation is significantly lacking. When it comes to imaging, state-of-the-art algorithms tend to use the Born-Iterative Method (BIM) and its variants [5]–[7]. However, these methods rely on E-fields the extraction of which can be very challenging. Instead, some recent works used S-parameter data for imaging, either through the use of Fréchet Derivatives [2], [8] or with a waveport vector Green's function [3].

In this work, we take a major step forward and explore the feasibility of conformal microwave imaging systems through simulations and measurements using S-parameters as MWI data. The rest of the paper is organized as follows. Section II presents the imaging configuration and algorithm. Section III reports simulation and measurement results. Section IV discusses the results with scopes for improvement.

II. Conformal Microwave Imaging with S-parameters

A. Imaging Configuration

The conformal imaging system consists of $N_a = 12$ half-wavelength dipole antennas, surrounding a hollow plastic frame or radius $10.5cm$. The antennas are evenly distributed along the circumference of the frame. Two dielectric cylinders of radius $1.5cm$ are 3D printed using a dielectric resin with $\epsilon_r \approx 3.4(1 - j0.05)$. The centers of the two cylinders are placed $10cm$ apart. The dipole antennas are connected to a network analyzer through a 50Ω switching matrix [9]. The complete configuration is shown in Fig. 1.

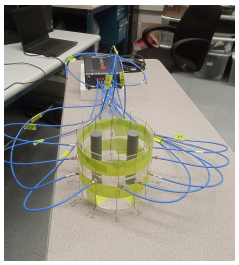

Fig. 1. Conformal imaging setup with cylindrical anomalies

For the 12 dipole antennas, we get a total $M = \frac{N_a(N_a-1)}{2} = 66$ independent measurements due to the reciprocity of the network; i.e: $S_{i,j} = S_{j,i}$, with i and j being the indices of the two antennas under consideration $(i = 1, 2, ...N_a, j = 1, 2, ...N_a)$ [4]. All data are collected at $1.8GHz$.

B. Imaging Algorithm

For imaging, we used the BIM algorithm [5] with Fréchet derivatives as data equations [8]. The BIM workflow is governed by the two matrix formulations:

$$\left[E_i\right]^{(k)} = \left[E_i^{(inc)}\right] - \left\{\left[G\right]\mathcal{D}(\left[\delta\epsilon\right])^{(k-1)}\left[E_i^*\right]^{(k-1)}\right\}^T \quad \text{(1a)}$$

$$\left[S_{i,j}\right] = \frac{-j\omega\epsilon_0 A}{2a_i a_j}\left[\delta\epsilon\right]^{(k)}\left\{\left[E_i\right]^{(k)} \odot \left[E_j\right]^{(k)}\right\} \quad \text{(1b)}$$

Here, the (k) superscript indicates the values of different quantities after iteration k; $\left[\delta\epsilon\right]^{(k)} \in \mathbb{C}^{N\times 1}$ is the complex dielectric contrast vector across N subdomains inside the object, which we are interested in reconstructing; $\left[E_i\right]^{(k)} \in \mathbb{C}^{M\times N}$

is the E field matrix which contains the complex E-fields inside each subdomain, the i subscript refers to the fields generated by the i^{th} antenna; $\mathbb{D}([.])$ is an operator to diagonalize a column matrix; $\left[G\right] \in \mathbb{C}^{N\times N}$ is the subdomain 2D Green's function matrix (sufficient since the dipole radiation is dominated by the TM polarization) [4]; $\left[S\right] \in \mathbb{C}^{M\times 1}$ is the received S parameter vector; A is the subdomain area; a_i, a_j are magnitudes of the power waves at antenna ports i, j respectively [8]; $\{.\}^T$ is the regular transpose for rearranging matrices properly; $\odot$ is the elementwise product; and $[.^*]$ is the conjugate transpose.

The BIM starts the iteration at $k = 0$ assuming $\left[E_i\right]^{(0)} = \left[E_i^{(inc)}\right]$. Here, $\left[E_i^{(inc)}\right] \in \mathbb{C}^{M\times N}$ is the matrix containing E-fields inside each subdivision without the presence of the anomaly. We can obtain this E-field from any prior simulation with the given locations of the antennas [3]. Next, each iteration starts with computing the forward solution (1a) using method of moments (MoM). (1b) is an ill-posed problem of the form $[y] = [A][x]$, which aims to solve $[x]$. We have used Truncated Landweber (TLW) [4] optimization to solve for the unknown quantity $\left[\delta\epsilon\right]^{(k)}$.

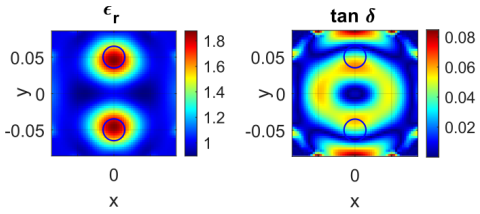

(a)

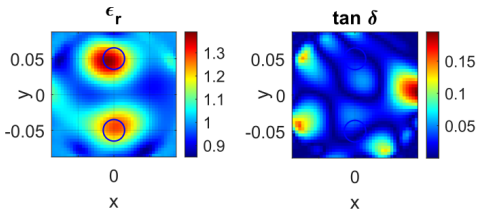

(b)

Fig. 2. Reconstructed dielectric constant (ϵ_r) and loss tangent ($\tan\delta$) values; (a) simulation in CST (b) measurement.

III. Results

We herewith present the reconstruction results from the measured S-parameters and compare them with simulation results obtained using the CST electromagnetic solver. Specifically, reconstructed images obtained from simulation and measurement results are shown in Fig.2. The simulation results show excellent localization of the reconstructed image, whereas reconstruction from the measurement has lower quality, and a slight offset in localization. During measurements, we observed unstable S-parameter curves, which may have contributed to the degraded quality. Furthermore, during measurements, the dipoles could not be placed exactly in the locations used for simulations, so the knowledge of $\left[E_i^{(inc)}\right]$ may not have been the optimal initialization for the iterations to commence. We also note that the simulation and measurement images contain some residual trace of the antenna locations, which we tried to minimize by applying a small 2D smoothing filter. Finally, even though the localization was quite good, the reconstructed magnitude falls behind the actual dielectric values. Due to the ill-posedness of the problem, we had to apply sufficient perturbation of the singular values during the TLW inversion with a truncation parameter [4], which has compromised quantitative information.

IV. Discussion and Conclusion

Despite experimental limitations, the images from simulation and measurement have provided good qualitative information on the location of the objects. The measurement instability may readily be mitigated with the use of chokes or baluns at the end of the cables. For more complex antennas with multiple polarization directions, the algorithm can be improved using the 3D Green's function. Future work involves exploring more complicated images with inhomogeneous separation at the antenna positions (e.g., by having the antenna frame contain biological phantoms instead). We expect the residual images of the antennas to become more prominent for the inhomogeneous scenarios, which will need careful analysis. A successful continuation and implementation of the conformal imaging system will contribute significantly in the diagnosis of biological anomalies using a wearable form factor.

Acknowledgment

This work was supported by the National Science Foundation under grant 2244882.

References

[1] C. A. Balanis, R. D. Radcliff, and H. W. Hill, "Radio-Frequency Imaging in Geophysical Applications," *Journal of Microwave Power*, vol. 18, no. 1, Jan. 1983.

[2] A. Fedeli, V. Schenone, A. Randazzo, M. Pastorino, T. Henriksson, and S. Semenov, "Nonlinear S-Parameters Inversion for Stroke Imaging," *IEEE Trans. Microwave Theory Techn.*, vol. 69, no. 3, pp. 1760–1771, Mar. 2021.

[3] Y. Fang, K. Bakian-Dogaheh, and M. Moghaddam, "Real-Time 3D Microwave Medical Imaging With Enhanced Variational Born Iterative Method," *IEEE Trans. Med. Imaging*, vol. 42, no. 1, pp. 268–280, Jan. 2023.

[4] M. Pastorino, *Microwave imaging*. John Wiley & Sons, 2010.

[5] Y. Wang and W. Chew, "An Iterative Solution of the Two-Dimensional Electromagnetic Inverse Scattering Problem," *International Journal of Imaging Systems & Technology*, vol. 1, no. 1, pp. 100–108, 1989, publisher: John Wiley & Sons, Inc.

[6] W. Chew and Y. Wang, "Reconstruction of two-dimensional permittivity distribution using the distorted Born iterative method," *IEEE Trans. Med. Imaging*, vol. 9, no. 2, pp. 218–225, Jun. 1990.

[7] N. Zaiping, Y. Feng, Z. Yanwen, and Z. Yerong, "Variational born iteration method and its applications to hybrid inversion," *IEEE transactions on geoscience and remote sensing*, vol. 38, no. 4, pp. 1709–1715, 2000.

[8] N. K. Nikolova, *Introduction to Microwave Imaging*, ser. EuMA High Frequency Technologies Series. Cambridge: Cambridge University Press, 2017.

[9] Keysight, "P9164C 2X16 USB Solid State Switch Matrix, 300 KHz to 18 GHz." [Online]. Available: https://www.keysight.com/us/en/product/P9164C/2x16-usb-solid-state-switch-matrix-300-khz-to-18-ghz.html